Prospects and Challenges for Touchless Sensing of Spacecraft Electrostatic Potential Using Electrons

Miles Bengtson, Joseph Hughes, and Hanspeter Schaub

***Abstract*— A method is investigated to use secondary electrons to touchlessly sense the electrostatic potential of an object in geosynchronous orbit or deep space. This method involves a positively charged servicing craft, which directs a high-energy electron beam at the object of interest such that low-energy secondary electrons are emitted from the surface. The low-energy electrons emitted by the target are accelerated toward the servicing craft and arrive with an energy equal to the potential difference between the two crafts. The servicing craft measures the electron energy spectrum and, knowing its own potential, then infers the potential of the target. Depending on the application, photoelectrons could similarly be used to infer the target potential without the need for an active electron beam. Though it is possible to measure potential by directly contacting a surface, remote measurement offers significant advantages and supports missions which must operate in close proximity without making physical contact. Several missions have been proposed that use interactions between charged objects to create useful forces and torques, including electrostatic detumbling and reorbiting of debris, Coulomb formations, and virtual structures. Remote measurement of potential would benefit these missions by enabling feedback control of the active charging. Other applications include mitigation of arcing during rendezvous, docking, and proximity operations for future servicing or salvaging missions.**

***Index Terms*— Space technology, satellite constellations, voltage measurement.**

I. Introduction

THOUGH spacecraft charging has been studied for decades, there is a lack of understanding of how to effectively sense and monitor the charge on a space object from a distance. Whereas it is possible for a satellite to measure its own charge using plasma instruments, little research has been done on touchlessly sensing the charge on another space object. This paper discusses the prospects and challenges of a promising method for remote sensing of the electrostatic potential of a nearby space object. This method involves measuring the energy distributions of electrons, which are emitted from the target object. Secondary electrons are generated when an energetic particle impacts a surface, and photoelectrons are both emitted from the conducting surface with only a few electronvolts kinetic energy. A closely coorbiting servicing satellite can achieve a high positive potential relative to the target to measure the initially low-energy electrons that are accelerated toward the servicing craft. The electrons arrive with an energy equal to the potential difference between the two craft plus their small emission energy. Therefore, by knowing the potential of the servicing craft, the potential of the target object is inferred. For forced charging applications, the servicing craft directs an electron beam at the target to generate the secondaries. For natural charging, photoelectrons emitted when the spacecraft is in sunlight allow the technique to be used passively. Fig. 1 shows a concept of operations for the proposed remote sensing technique. The ability to remotely sense spacecraft potential has a broad range of applications. As electrical discharges and arcs between differentially charged surfaces can be detrimental to satellite components, remote potential sensing could be used for on-orbit experiments to better understand differential charging and subsequent arcing, thereby allowing electrostatic-related anomalies or mission failures to be mitigated. There is a similar risk of electrostatic discharge for proximity operations and docking with uncharacterized objects, which may float at different potentials [1]. Carruth *et al.* [2] identified that, without proper precautions, a discharge could occur between an astronaut on an extravehicular activity and a large space structure, which would be fatal to the astronaut [3]. Therefore, the ability to measure the electrostatic potential on various objects from a distance will be important for missions involving rendezvous, docking, or proximity operations.

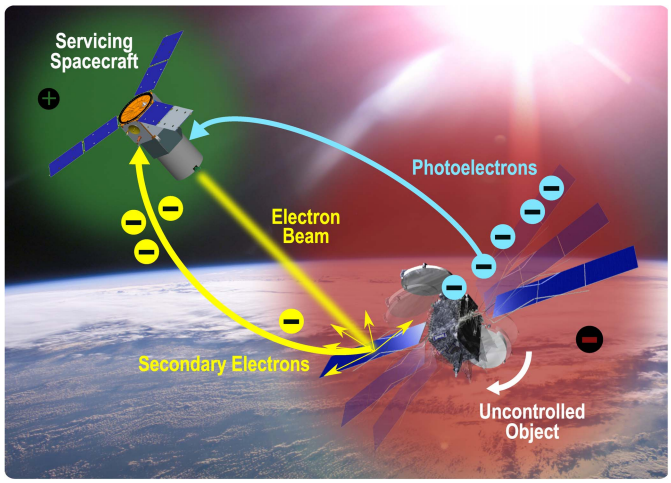

Fig. 1. Servicing craft observes the secondary electrons and photoelectrons emitted by a target object to touchlessly sense the object's electrostatic potential.

Manuscript received October 2, 2018; revised February 20, 2019; accepted March 27, 2019. Date of publication May 2, 2019; date of current version August 9, 2019. This work was supported by the National Defense Science and Engineering Graduate Fellowship. The review of this paper was arranged by Senior Editor H. B. Garrett. *(Corresponding author: Miles Bengtson.)*

M. Bengtson and H. Schaub are with the Aerospace Engineering Sciences Department, University of Colorado at Boulder, Boulder, CO 80309 USA (e-mail: miles.bengtson@colorado.edu; hanspeter.schaub@colorado.edu).

J. Hughes is with ASTRA, Louisville, CO 80027 USA (e-mail: jhughes@astraspace.net).

Color versions of one or more of the figures in this paper are available online at http://ieeexplore.ieee.org.

Digital Object Identifier 10.1109/TPS.2019.2912057

0093-3813 © 2019 IEEE. Personal use is permitted, but republication/redistribution requires IEEE permission.
See http://www.ieee.org/publications_standards/publications/rights/index.html for more information.

Though spacecraft charging has historically been viewed as a hazard to be mitigated, in recent years, many studies have investigated leveraging charged spacecraft to enable novel mission architectures. Missions are being proposed in which several smaller satellites flying in formation can accomplish tasks, which would be difficult or impossible for a single, monolithic spacecraft [4]. The Coulomb forces between multiple charged spacecraft can be used to create formations and virtual structures, which require no traditional propellant [5]–[8]. Another concept involves using electrostatic forces to inflate membrane structures [9], [10]. As valuable orbital regions become increasingly congested with retired satellites and hazardous debris, the need for active debris removal has been firmly established [11], [12]. The electrostatic tractor (ET) is an elegant method, which uses electrostatic forces to raise the orbits of debris at geosynchronous orbit (GEO) to a graveyard orbit or detumble uncooperative objects without making physical contact [13], [14]. In addition, satellite operators are looking to maximize the use of assets in orbit and orbital servicing concepts have been proposed for refueling, repair, or replacement of components. Such missions may enable satellite lifetimes to be extended or new satellites to be assembled from salvaged components [15]–[17]. These concepts, which are significant areas of research for future space operations, require close proximity operations, rendezvous and docking, knowledge of a nearby object's characteristics, and/or physical contact. Touchless potential sensing systems can fill a key gap in current knowledge of spacecraft charging, allowing for a better understanding of the negative impacts of undesired charging and significantly advancing the possible uses for electrostatics in space.

Though spacecraft charging has been studied extensively, little work has been done on the topic of remote sensing of charge. Ferguson *et al.* [18] propose the concept of remote sensing of charging or arcing and consider various techniques to remotely monitor high-level charging or arcing events on satellites, including surface glows, bremsstrahlung X-rays, and radio or optical emission from arcing. Bennett [19] discusses how the charge on one satellite in a two-craft formation can be estimated from the relative motion dynamics, which are driven by the Coulomb force using range and range rate measurements. However, this method only provides an estimate of the electrostatic potential with low spatial and temporal resolution. Engwerda *et al.* [20] propose a method for sensing charge by directly measuring the electric field around an object. This paper focuses on how to use the voltage measurements to obtain a charge estimate and then develop a multisphere electrostatic model of the target [21], but does not consider the challenges of obtaining a direct electric field measurement near a charged object in plasma.

Halekas et al. [22], [23] use secondary electrons and photoelectrons measured by the Lunar Prospector spacecraft to remotely map the charge distribution on the surface of the Moon. The measurements were completely passive, with the low-energy electrons being generated by solar photons or plasma currents. In addition, the authors compare the incident currents with the secondary currents to estimate the secondary electron yield of lunar regolith [24]. This reference demonstrates the feasibility of remotely mapping the charge and characterizing the material properties of a surface using electrons.

It should be emphasized that the proposed technique does not require the development of new hardware, but rather uses existing satellite detector systems in a novel way to obtain new information. In the simplest operation, the touchless sensing concept requires only an electron energy analyzer on the servicing craft. Such instruments have extensive flight heritage in space science missions ([25]–[28]). Furthermore, both the U.S. Air Force and the European Space Agency have developed standardized energetic particle detectors to act as a radiation monitors and collect data for space weather models [29], [30]. As of 2015, all new Air Force satellites are required to integrate an energetic charged particle sensor [31]. Therefore, numerous satellites are already in orbit and more will be launched, which possess the ability to measure electron energy distributions.

This paper presents prospects and challenges for using secondary electrons to touchlessly sense the potential of a closely neighboring space object. This paper is outlined as follows. Section II provides the theory of secondary and photoelectron emission and also discusses challenges of remote potential sensing. In Section III, computer simulations are used to investigate the trajectories of electrons in the vicinity of charged spacecraft. The effects of various geometries, relative distances, and potentials on the charge sensing method are considered. Two case studies are presented in Sections IV and V to demonstrate the feasibility of the concept.

II. Theory and Concept

A. Secondary Electron Emission

When a primary electron impacts a surface, it liberates electrons that leave the surface with a spectrum of energies. By convention, electrons that leave the surface with less than 50 eV are called secondary electrons. Those with energies from 50 eV up to the incident energy are called backscattered electrons. The energy distribution of backscattered electrons has a peak near the incident beam energy and that of secondary electrons has a peak at several electronvolts, regardless of the incident beam energy. Fig. 2(a) shows a schematic of how secondary electrons are generated by an energetic particle impacting the surface. Fig. 2(b) shows an example secondary electron yield curve. The secondary electron coefficient or yield, δ, is the probability that a secondary electron will be emitted for every primary electron that strikes the surface. This coefficient is a function of the primary electron energy and is different for every material. For many materials, the secondary electron coefficient exceeds unity for a given energy range. This implies that for every primary electron, multiple secondary electrons are emitted. Several common models for the secondary electron yield are given in [32] and [33]. By convention, secondaries have energies less than 50 eV, whereas backscattered electrons have energies greater than 50 eV and close to the incident beam energy [34]. Secondary electron energy distributions show that most secondaries are emitted with energies less than 10 eV [35]. The

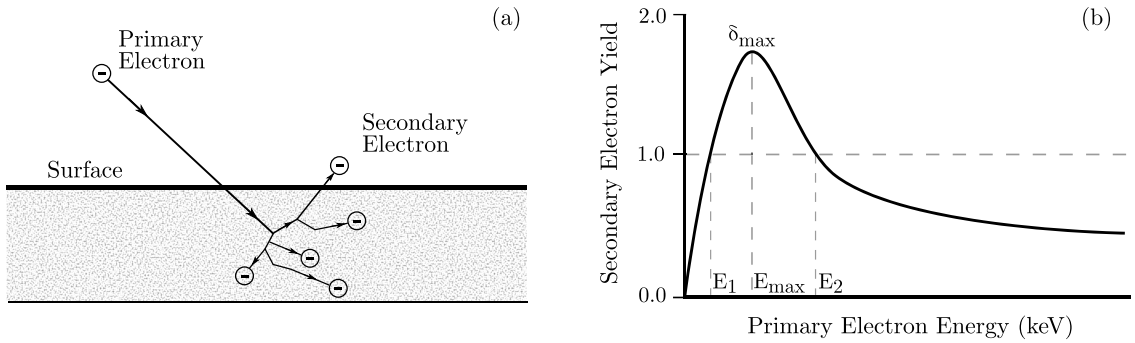

Fig. 2. (a) Depiction of secondary electron generation. (b) Example secondary electron yield curve.

Chung–Everhart model describes the energy distribution of emitted secondary electrons

$$f(E) = \frac{(E - E_F - \Phi)}{(E - E_F)^4} \tag{1}$$

where E is the energy of the emitted electron, E_F is the Fermi energy, and Φ is the work function of the metal surface [36]. Secondary electrons are emitted from a surface with a cosine angular distribution about the surface normal that is independent of the angle of incidence of the primary electron [35]. The secondary yield, however, increases with increasing incidence angle because more energy from the primary electron is deposited near the surface where secondaries have a high probability of escape.

B. Photoelectron Emission

Energy from the sun can energize electrons in the first few nanometers of the spacecraft so that they leave the surface. The current is given by

$$I_p = \begin{cases} j_{\text{ph}} A e^{-q\phi/k_B T_{\text{ph}}} & \phi > 0 \\ j_{\text{ph}} A & \phi \leq 0 \end{cases} \tag{2}$$

where j_{ph} is the photoelectron flux, A is the sunlit area, and $k_B T_{\text{ph}}$ is the thermal energy of the ejected photoelectrons [37]. For aluminum, $k_B T_{\text{ph}} = 2$ eV and $j_{\text{ph}} = 40\ \mu\text{A/m}^2$. For a negative spacecraft, this current is constant, and for a positive spacecraft, it quickly vanishes. Most of the photoelectrons will be recaptured if the target is positive, so it may be challenging to measure the positive potentials unless the sensing craft is very positive.

C. Remote Sensing Using Electrons

Remote potential sensing is enabled by the fact that secondaries and photoelectrons are emitted with very low energy. Therefore, the electron energy measured at the servicing craft is approximately equivalent to the potential difference between the two craft.

Spacecraft surface charging is frequently discussed in the context of GEO. In dense plasmas, such as those in low Earth orbit (LEO), the ambient plasma density is sufficiently large that there will be thermal collisions between the secondary or photoelectrons. Similarly, the electric field between the two craft will be shielded out over short distances. Thus, the proposed technology is better suited to tenuous plasmas such as that found at GEO or in deep space.

The relative motion between the two craft evolves with timescales of seconds or minutes. Given separation distances of tens of meters, the electrons are transported between the two craft on the order of microseconds. Detection instruments that measure the electrons typically have response times on the order of milliseconds. Therefore, the sensing method is sufficient to provide real-time closed-loop control for Coulomb actuation missions.

There are several challenges associated with using electrons for remote sensing. The first challenge is to ensure that a sufficient signal is obtained from the secondary or photoelectron current such that it is observable by an instrument relative to the ambient plasma population. The electric field about a charged object falls off with the distance squared, so beyond some distance, the electrons of interest will be affected by environmental fields and will no longer be distinguishable from background fluxes. This imposes requirements that the sensing craft is able to fly in proximity to the target object. Depending on the method of sensing and relative geometry, the sensing craft may need to operate within several craft radii of the target object. However, servicing, salvaging, docking, and remote actuation missions already propose flying in close proximity. Future studies will investigate the maximum distance at which the charge on an object can be sensed under various environmental conditions.

A similar challenge arises related to obtaining a sufficient number of electrons to measure. For forced charging applications, such as the ET, an active electron beam is directed at the target, which generally dominates the other currents to and from the object. Therefore, a large number of secondaries are generated which can be measured. For natural charging applications, the photoelectric current often dominates and therefore produces a large number of electrons which can be measured. However, if an electron beam is not used, the servicing craft must achieve a relative orbit such that it can observe the escaping photoelectrons. In other words, it must be on the sunlit side of the target object, which further imposes requirements on the mission. If the photoelectric current is not present at all (for example, in eclipse), it may be possible to use a short pulse from an electron beam to generate secondary electrons. A concern is how to generate secondaries without changing the charge state of the target which the servicing craft is attempting to measure. Future studies will

investigate this and also whether secondaries generated by ambient plasma fluxes could be used for passive sensing of electrostatic potential.

Another challenge arises from the fact that spacecraft is composed of various components, which may float at different potentials. Therefore, the electric field geometry about the spacecraft may be complex, with potentials wells and barriers, which make it difficult to measure the emitted secondary electrons. In addition, the sensing system may measure different peaks in the electron energy distribution associated with the differentially charged components. A sufficient spatial resolution of the sensing system is required to resolve the potentials of each component. As each material has unique secondary emission properties, there is a possibility for multiple electron populations from spacecraft components with different materials and charge states. Finally, dielectrics and insulators, which are common on spacecraft surfaces, have different charging and secondary emission physics than that of conductors. Future work will investigate how the remote sensing technique can be implemented for realistic spacecraft materials and geometries.

The primary question to be investigated in the remainder of this paper is under what conditions a sufficient number of secondary electrons are captured to measure the charge of the target object. The following section describes the development and results of numerical studies used to investigate this question.

III. Simulation and Results

A. Simulation Setup

A 2-D simulation was written in Matlab to analyze the feasibility for using low-energy electrons to remotely sense the charge of an object in space. Initially, each spacecraft was modeled as a single sphere so that the electric field can be computed straightforwardly. Voltages are assigned to the servicing craft and target object and then the charges are computed using the capacitance matrix [21], [38], [39] as

$$\begin{bmatrix} q_S \\ q_T \end{bmatrix} = [C(\rho)] \begin{bmatrix} \phi_S \\ \phi_T \end{bmatrix} \tag{3}$$

$$[C(\rho)] = \frac{\rho}{k_c(\rho^2 - R_S R_T)} \begin{bmatrix} R_S\rho & -R_S R_T \\ -R_S R_T & R_T\rho \end{bmatrix} \tag{4}$$

where $[C(\rho)]$ is the 2×2 capacitance matrix, ϕ_S and ϕ_T are the servicing craft and target object voltages, respectively, q_S and q_T are the charges, R_S and R_T are the object radii, ρ is the center-to-center separation distance, and k_c is the Coulomb constant.

The total electric field at a given point is found by the following equation:

$$\boldsymbol{E} = k_c \frac{q_S \boldsymbol{r}_S}{r_s^3} + k_c \frac{q_T \boldsymbol{r}_T}{r_T^3} \tag{5}$$

where $\boldsymbol{r}_S$ and $\boldsymbol{r}_T$ are the distances from the given point to the center of the servicing craft and target object, respectively. The force on each electron is computed at each timestep using the combined electrostatic and Lorentz force

$$\boldsymbol{F} = q(\boldsymbol{E} + \boldsymbol{v} \times \boldsymbol{B}) \tag{6}$$

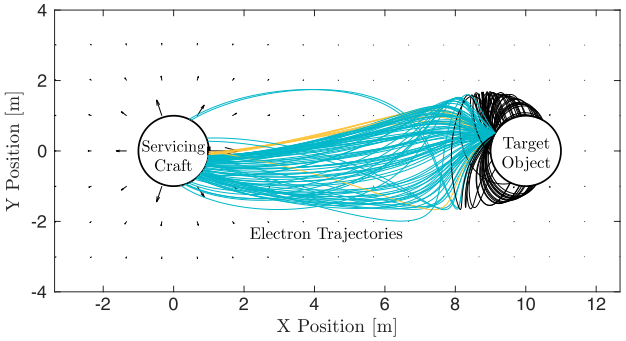

Fig. 3. Simulation results for an application with low charging levels and passive sensing. The electrons with black trajectories do not escape the target object's potential well, those with blue trajectories impact the servicing craft, and those with gold trajectories enter a 25 cm^2 detector on the front of the servicing craft. The black arrows denote the direction and relative magnitude of the electric field.

where q is the electron charge, $\boldsymbol{v}$ is the velocity of each particle relative to the magnetic field, which corotates with earth, and $\boldsymbol{B}$ is the magnetic field. For these simulations, a magnetic field strength of 100 nT directed out of the simulation plane was selected to represent the field at GEO, though the effect is very small. Mutual repulsion between electrons and effects of beam expansion into a vacuum are neglected. The spacecraft is assumed to be perfectly geostationary so the velocity of the electrons with respect to the spacecraft is also the velocity with respect to the B-field. A user-specified number of electrons are generated with initial energies of 5 eV at the surface of the target and an initial velocity distribution consistent with the cosine distribution relative to the local surface normal. At each timestep, the electric field is computed at each particle, then the forces are used to compute the next state using a fourth-order Runge–Kutta method with a variable timestep. Individual electrons that impact either craft or leave the simulation domain are stopped. At the conclusion of the simulation, the electrons that hit either the servicing craft or a designated sensor on the servicing craft are counted. This allows the fraction of detected particles to be computed and thus provides insight into the expected signal-to-noise ratio, as is discussed later on.

Fig. 3 shows an example of the simulation results for a case where a 1-m radius target object is charged to +20 V, the 1-m radius servicing craft to +100 V, and the two crafts are separated by 10 m. The particles are generated 0.5 m above the x-axis on the target object. Because the target is slightly positive, some of the secondary electrons (black trajectories) do not have the energy to escape the potential well and thus return to the target. Other electrons escape the target object and impact the servicing craft (blue trajectories), and a small number (gold trajectories) enter a 25 cm^2 sensor on the front of the servicing craft. This simulation demonstrates that even if the target object is charged positively, the servicing craft can measure the energy of the secondary electron population, as long as it is more positive than the target.

Fig. 4 shows results for a case simulating the operation of the ET so that both crafts achieve potentials with very large magnitudes. In this simulation, the servicing craft is charged to

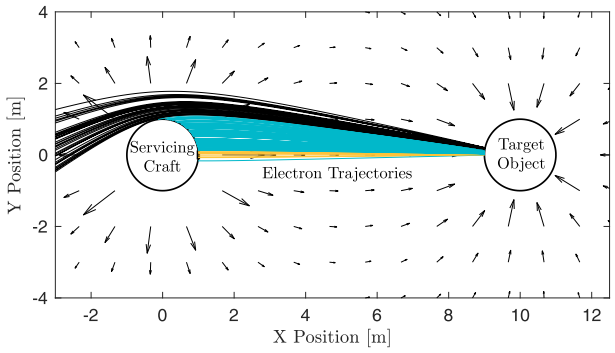

Fig. 4. Simulation results for an application with high, forced charging levels, and active sensing. The electrons with black trajectories escape into space, those with blue trajectories impact the servicing craft, and those with gold trajectories enter a 25 cm^2 detector on the front of the servicing craft. Black arrows: direction and relative magnitude of the electric field.

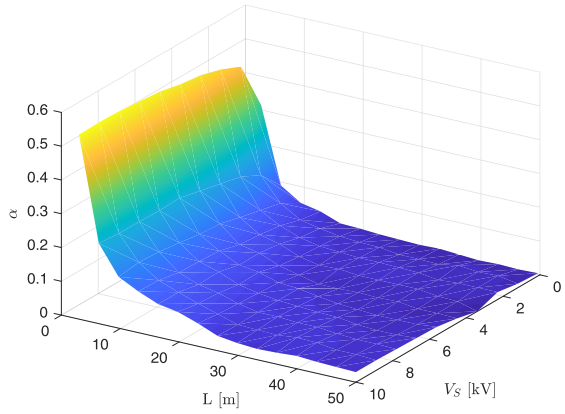

Fig. 5. Value of α as a function of separation distance and servicing craft voltage.

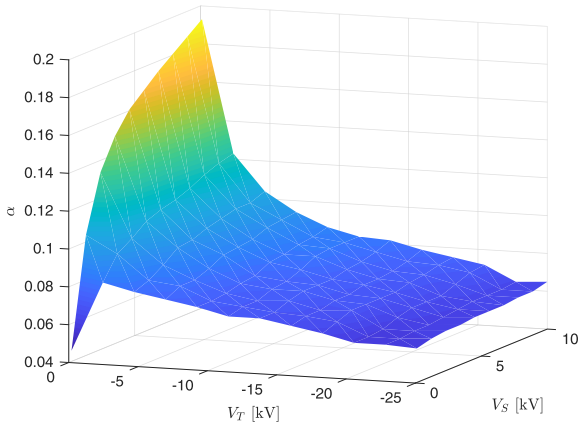

Fig. 6. Value of α as a function of the target object and servicing craft voltages.

+20 kV, the target object is charged to −20 kV, and electrons are generated on the target between 0 and 20 cm above the y-axis. Since both the active electron beam and secondary electron current occupy the same region near the centerline between the two crafts, it is assumed that these oppositely directed currents do not interfere with each other. Recent experimental work to validate the sensing concept confirms that this assumption is valid [40]. The experimental data show no significant interactions between the two beams, even at nearly antiparallel configurations. Again, the simulation confirms that the electrons arrive at the servicing craft with energies of approximately 40 keV. For applications with such high charging levels, there is a much smaller region on the target for which electrons will map onto the sensing detector.

B. Parameter Trade Studies

An important quantity for determining the feasibility of the proposed method is the fraction, α, of the emitted secondary electron current, I_{SEE}, which is captured by the detector on the servicing craft, I_{SEC}. This fraction is a function of the object potentials, the separation distance, and the relative geometry between the two crafts. A broad range of simulations have been run to investigate this parameter space and determine the conditions for which the secondary electron method for remote potential sensing may be feasible. Fig. 5 shows the fraction α plotted as a function of the servicing craft voltage, V_S, and the separation distance, L. In this simulation, the target object voltage, V_T, is held fixed at −100 V. Both crafts are assumed to be spheres of radius 1 m, the detector on the servicing craft is defined to be 25 cm^2, and the secondaries are generated along a 40 cm^2 area on the target object surface centered about the line of separation. The results show that the captured current depends most significantly on the separation distance. For separation distances of a few craft radii, the captured current is tens of percent of the emitted current. Beyond 10-m separation, the captured current decreases from 10 to a few percents of the emitted current. For forced charging applications where I_{SEE} is large, the remote potential sensing method would be feasible at operating distances of 10 s of meters. For other applications where I_{SEE} is small, it may be necessary to operate at separations of a few craft radii to obtain a sufficient signal-to-noise ratio. Sections IV and V provide case studies for specific operating conditions within each regime.

Fig. 6 shows how α depends on the voltage of both the servicing and target craft. The separation distance is fixed at 10 m and the same assumptions regarding the initial condition of the secondaries and the detector size are made again here. The highest value of α occurs when V_T is at the lowest magnitude potential and V_S is at the highest. This occurs because the electrons are not strongly accelerated away from the target at which they are generated, but are strongly accelerated toward the servicing craft. Therefore, the servicing craft collects a large fraction of the secondaries. Conversely, when V_T is large negative and V_S is small positive, α is very small. In this case, the electrons gain most of their energy when leaving the target surface and their trajectories are essentially determined before they are influenced by the servicing craft electric field. Therefore, only those electrons that are accelerated along the line between the two crafts will be captured by the detector. Interestingly, α is lowest where both V_T and V_S are small in magnitude. In this case, the electrons are not accelerated strongly and therefore travel slowly away from the target

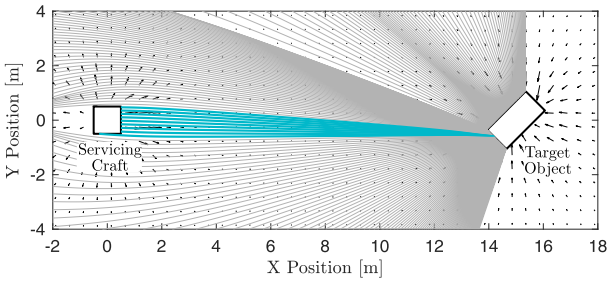

Fig. 7. Simulation results for two nonspherical spacecraft. The electrons with gray trajectories escape into space, those with blue trajectories impact the servicing craft. The target object is charged to −20 kV and the servicing craft is charged to +20 kV.

surface. Therefore, the initial velocities of the electrons are important and the initial cosine angular distribution has time to expand such that only a small percentage of the secondaries map onto the detector.

C. Rectangular Spacecraft Study

Another simulation was run to investigate the trajectories of electrons around charged spacecraft with more realistic and geometrically complex shapes. The method of moments (MOM) was used to find the electric field in the vicinity of the two spacecrafts due to the voltage of both of them. The MOM is an elastance-based method, which translates the voltage to charge on every node through an extension of Poisson's law [41]. Once the charge is found every node, the E-field can be computed at an arbitrary point in space.

For this simulation, a 1 m^3 is charged to +20 kV and a 2×1 m rectangular box charged to −20 kV is 15 m away and rotated by 45°. 144 polygons are used per square meter and the E-field is computed at 900 points in the xy plane. This E-field is then interpolated for trajectories that do not lie directly on the field points.

Fig. 7 shows the results of this paper. In this simulation, electrons are generated on every surface of the target, which is visible to the servicing craft. When the target is charged to potentials in the kilovolts range, the electrons will quickly reach high velocities as they fly away from the surface. Therefore, their trajectories are mostly determined by the field geometry at the target object and are not influenced significantly by the servicing craft. As shown in the figure, there is a small region on the target from which the electric field points to the servicing craft and the electrons make it to the craft (these trajectories are colored blue). By expanding the electron beam size such that it illuminates the entire target, it is possible to guarantee that some secondary electrons on the target will always map back to the servicing craft. Future research will investigate the sensing performance given more complex spacecraft geometries and the effects of a tumbling target.

IV. Case Study for Electrostatic Tractor

To demonstrate the feasibility of remote potential sensing, a case study was carried out with application to the ET. Reference [42] provides an example operating condition for the ET: a tractor of 2-m radius is charged to 21.4 kV, a debris object of radius 0.935 m is charged to −14.6 kV with a separation distance of 12.5 m. The electron beam energy is $E_{\mathrm{EB}} = 40$ keV and the beam current is $I_{\mathrm{beam}} = 520$ μA. Furthermore, it is assumed that the beam diameter is 20 cm and the beam impacts the target sphere centered on the line of separation. The secondary electrons are initialized with a kinetic energy of 5 eV and a cosine angular distribution. The trajectories of 2000 particles are simulated. The secondary electron emission current model is given by

$$I_{\mathrm{SEE}} = -4\delta_M I_{\mathrm{beam}} \kappa \tag{7}$$

where

$$\kappa = \frac{E_{\mathrm{eff}}/E_{\mathrm{max}}}{(1 + E_{\mathrm{eff}}/E_{\mathrm{max}})^2} \tag{8}$$

and

$$E_{\mathrm{eff}} = E_{EB} - q\phi_S + q\phi_T \tag{9}$$

δ_M is the peak of the secondary electron yield curve and E_{max} is the energy at which this peak occurs [43]. Values of $\delta_M = 1$ and $E_{\mathrm{max}} = 300$ eV are assumed, so $I_{\mathrm{SEE}} = 163$ μA.

The secondary electron current captured by the detector on the servicing craft, I_{SEC}, is found by

$$I_{\mathrm{SEC}} = \alpha I_{\mathrm{SEE}} \tag{10}$$

where α is between 0 and 1. For these conditions, the numerical simulation results show that 15.3% of the secondary electrons are captured by the 25 cm^2 detector centered on the tractor satellite. Therefore, $\alpha = 0.153$ and $I_{\mathrm{SEC}} = 25.0$ μA.

The flux of secondary electrons occurs at a very narrow range of energies corresponding to the potential difference between the two crafts plus the initial energy distribution of the electrons. The captured secondary current is converted to a flux so that it can be compared to the ambient electron flux. The captured secondary flux, F_{SEC}, is modeled as a population distributed according to the Chung–Everhart model. Values of 11.7 and 4.08 eV are assumed for the Fermi energy and work function, respectively. Fig. 8 shows the secondary electron flux superimposed on a bi-Maxwellian background. The bi-Maxwellian model parameters were selected to be representative of storm-time conditions in GEO, with $n_1 = 0.3$ cm^{-3}, $T_1 = 4$ keV, $n_2 = 0.2$ cm^{-3}, and $T_2 = 7$ keV [44]

$$F = \sum_{i=1}^{2} n_i \sqrt{\frac{q}{2\pi T_i m_e}} \frac{q\phi_S}{k_B T_i} \exp\left(\frac{q\phi_S}{k_B T_i}\right) \tag{11}$$

where k_B is Boltzmann's constant and m_e is the electron mass. Fig. 8 shows the electron flux at the sensing craft, including both the ambient plasma and the secondary electron population. The dashed black line shows the expected value of the secondary population energy, equal to $\phi_S - \phi_T = 36.0$ keV. The response of a realistic energetic particle detector to the secondary electron population is modeled. Numerous electron energy analyzers have been utilized in laboratory and on-orbit

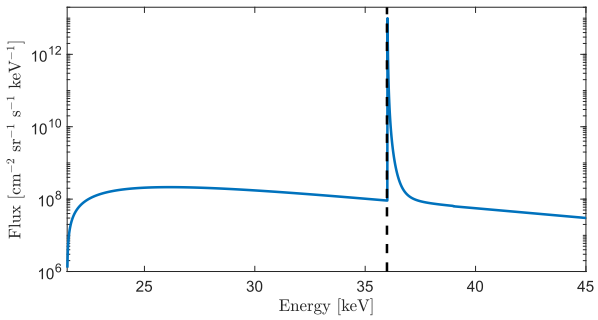

Fig. 8. Electron fluxes for the ET remote potential sensing case study. The background fluxes are a bi-Maxwellian and the peak is the secondary electron signal. The dashed black line represents the expected energy value.

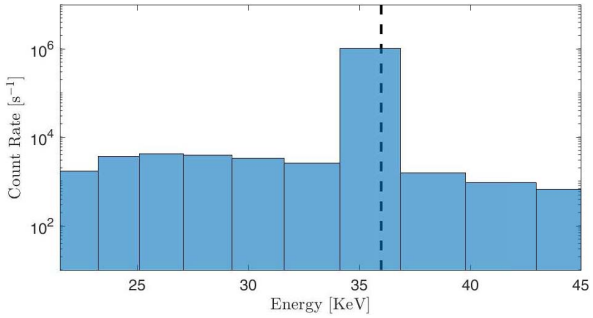

Fig. 9. Model of observed electrostatic analyzer signal for the ET remote potential sensing case study, in which the fluxes have been binned assuming an instrument resolution of 8%.

missions. Electrostatic analyzer-type instruments use electric fields to filter between particles of different energies [26]–[28], [45], [46]. These detectors can measure energies ranging from a few electronvolts to tens of kiloelectronvolts (30–50 keV typical) and have energy resolutions of $\Delta E/E = 2$–15%. At higher energies, electron telescopes use stacks of silicon detectors to measure the energy distribution of electrons [47], [48]. Silicon detectors can measure energies ranging from tens of kiloelectronvolts to megaelectronvolts with energy resolutions comparable to those of electrostatic analyzers. Both types of particle detectors can be used in parallel so a given spacecraft can measure across a wide range of energies with good resolution.

To model the response of an instrument, it is assumed that the instrument can measure in the range of 30 keV with an energy resolution of $\Delta E/E = 8\%$ and a geometric factor of 2×10^{-5} cm^2 sr keV (comparable to that in [45]). Fig. 9 shows the count rates, which would be observed by an instrument with these parameters. The dashed black line indicates the actual value of the electron energy peak (36.0 keV). The energy bin which ranges from 34.1 to 36.9 keV is several orders of magnitude higher than the background. This is because the detected secondary electron current is already large, and further, the secondary electrons are limited to a very narrow energy range. Even for geometries in which the majority of the secondary electrons escape into space, the signal peak from a small percentage of captured electrons provides sufficient information for the potential of the target object to be determined. Subtracting the potential of the servicing craft from the bin edges of the electron peak gives a range of values for the target potential between 12.7 and 15.5 keV or an accuracy of 6%–13%. Using an instrument with finer energy resolution would reduce these values. In light of these results, the proposed method for remote potential sensing is feasible for the ET application given current capabilities.

V. Case Study for Passive Sensing Applications

Another case study is presented to determine the feasibility of passive sensing of potential using photoelectrons. An operating condition is assumed in which the sensing craft and target object are spheres of 1-m radius, separated by 8 m, with $\phi_S = 200$ V and $\phi_T = -50$ V. The target is assumed to be a conducting, aluminum sphere with $j_{\rm ph} = 40$ μA/m^2 and $k_B T_{\rm ph} = 2$ eV. The electrons are again given an initial cosine angular distribution. It is assumed that the half of the target sphere facing the servicing craft is in sunlight. Under these conditions, only 1.75% of the emitted photoelectrons are captured by the sensor on the servicing craft. This percentage is small because photoelectrons are generated on a large area of the target craft, but only a small area maps back to the sensor. Assuming the sunlit area is a circle, the emitted photoelectron current is 126 μA. Given $\alpha = 0.175$, the current captured by the servicing craft sensor is 2.2 μA. As in the previous section, the photoelectron population is modeled as a Maxwellian distribution with a temperature of 1.5 eV [49]. The same bi-Maxwellian distribution used in the previous section is used again here for the ambient plasma. Fig. 10 shows the photoelectron population flux superimposed on the bi-Maxwellian background. The dashed black line indicates the potential difference between the two spacecrafts. The peak photoelectron flux is several orders of magnitude larger than the background flux, therefore the signal is easily detectable given current energy analyzer capabilities. In light of this result, touchless potential sensing is feasible for passive sensing applications in which only photoelectrons are used.

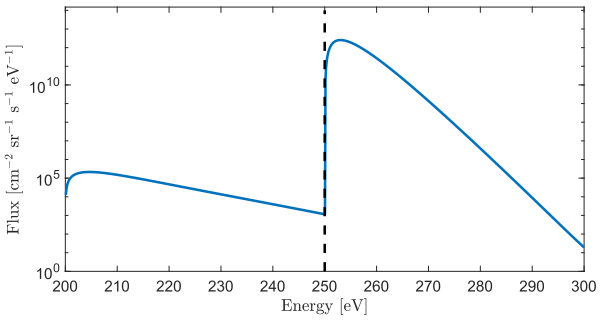

Fig. 10. Electron fluxes for the photoelectron remote potential sensing case study. Black dashed line: expected energy value of the photoelectrons. Note that units of eV are used instead of keV. The background plasma is modeled as a double-Maxwellian representative of GEO conditions.

VI. Conclusion

This paper presents the prospects for how electrons can be used to touchlessly sense the charge on a space object, as well as the challenges for further development. Using either secondaries from an active electron beam or the photoelectron

current, the potential on an object can be sensed over distances of tens of meters in GEO with realistic instrumentation. Several challenges are identified, which will be addressed in future work. Realistic spacecraft geometries may produce potential wells and barriers that complicate the measurement. Similarly, the sensing of charge for differentially charged spacecraft may not be straightforward. Open questions include how incorporating more sophisticated electrostatic and secondary electron emission models impacts the sensor performance. Future work will also consider if the target surface material can be identified from the secondary electron characteristics measured during the sensing process. Laboratory experiments both in vacuum and in plasma are planned to demonstrate the concept with a variety of materials, geometries, and charge regimes, and also validate the numerical results.

ACKNOWLEDGMENT

The authors would like to thank J. Maxwell, K. Wilson, R. Hoffman, and Z. Sternovsky for fruitful discussions on this topic.

REFERENCES

[1] D. Barnhart *et al.*, "Phoenix program status—2013," in *Proc. AIAA Space Conf. Expo.*, 2013, p. 5341.

[2] M. Carruth, Jr., *et al.*, "Iss and space environment interactions without operating plasma contactor," in *Proc. 39th Aerosp. Sci. Meeting Exhib.*, 2001, p. 401.

[3] D. Ferguson, T. Morton, and G. Hillard, "First results from the floating potential probe (FPP) on the international space station," in *Proc. 39th Aerosp. Sci. Meeting Exhib.*, 2001, p. 402.

[4] M. Martin and M. Stallard, "Distributed satellite missions and technologies—The techsat 21 program," in *Proc. Space Technol. Conf. Expo.*, 1999, p. 4479.

[5] L. B. King, G. G. Parker, S. Deshmukh, and J.-H. Chong, "Spacecraft formation-flying using inter-vehicle coulomb forces," NASA/NIAC, Washington, DC, USA, Tech. Rep., Jan. 2002.

[6] H. Schaub and L. E. Z. Jasper, "Orbit boosting maneuvers for two-craft coulomb formations," *AIAA J. Guid., Control, Dyn.*, vol. 36, no. 1, pp. 74–82, Jan./Feb. 2013.

[7] H. Joe, H. Schaub, and G. G. Parker, "Formation dynamics of coulomb satellites," in *Proc. 6th Int. Conf. Dyn Control Syst. Struct. Space*, Riomaggiore, Italy, Jul. 2004, pp. 79–90.

[8] H. Schaub, G. G. Parker, and L. B. King, "Challenges and prospects of coulomb spacecraft formations," *Adv. Astron. Sci.*, vol. 115, no. 1, pp. 169–193, Jan. 2004.

[9] L. A. Stiles, H. Schaub, K. K. Maute, and D. F. Moorer, "Electrostatically inflated gossamer space structure voltage requirements due to orbital perturbations," *Acta Astronautica*, vol. 84, pp. 109–121, Mar./Apr. 2013. [Online]. Available: http://www.sciencedirect.com/science/article/pii/S0094576512004584

[10] L. A. Stiles, H. Schaub, K. Maute, and D. F. Moorer, "Electrostatic inflation of membrane space structures," in *Proc. AAS/AIAA Astrodynamics Spec. Conf.*, Toronto, ON, Canada, Aug. 2010, p. 8134.

[11] P. V. Anderson and H. Schaub, "Local debris congestion in the geosynchronous environment with population augmentation," *Acta Astronautica*, vol. 94, no. 2, pp. 619–628, Feb. 2014.

[12] H. Schaub, L. E. Z. Jasper, P. V. Anderson, and D. S. McKnight, "Cost and risk assessment for spacecraft operation decisions caused by the space debris environment," *Acta Astronautica*, vol. 113, pp. 66–79, Aug./Sep. 2015.

[13] H. Schaub and D. F. Moorer, Jr., "Geosynchronous large debris reorbiter: Challenges and prospects," *J. Astron. Sci.*, vol. 59, nos. 1–2, pp. 161–176, 2012.

[14] T. Bennett, D. Stevenson, E. Hogan, and H. Schaub, "Prospects and challenges of touchless electrostatic detumbling of small bodies," *Adv. Space Res.*, vol. 56, no. 3, pp. 557–568, 2015.

[15] D. A. Whelan, E. A. Adler, S. B. Wilson, and G. M. Roesler, "DARPA orbital express program: Effecting a revolution in space-based systems," *Proc. SPIE*, vol. 4136, Nov. 2000, pp. 48–57.

[16] A. Ellery, J. Kreisel, and B. Sommer, "The case for robotic on-orbit servicing of spacecraft: Spacecraft reliability is a myth," *Acta Astronautica*, vol. 63, nos. 5–6, pp. 632–648, 2008.

[17] B. Sullivan *et al.*, "DARPA phoenix payload orbital delivery system (PODs): 'FedEx to GEO'," in *Proc. AIAA SPACE Conf. Expo.*, 2013, p. 5484.

[18] D. C. Ferguson, J. Murray-Krezan, D. A. Barton, J. R. Dennison, and S. A. Gregory, "Feasibility of detecting spacecraft charging and arcing by remote sensing," *J. Spacecraft Rockets*, vol. 51, no. 6, pp. 1907–1913, 2014.

[19] T. J. Bennett, "On-orbit 3-dimensional electrostatic detumble for generic spacecraft geometries," Ph.D. dissertation, Dept. Aerosp. Eng. Sci., Univ. Colorado Boulder, Boulder, CO, USA, 2017.

[20] H. J. A. Engwerda, J. Hughes, and H. Schaub, "Remote sensing for planar electrostatic characterization using the multi-sphere method," in *Proc. Stardust Final Conf. ESTEC*, Amsterdam, The Netherlands, Oct. 2016, pp. 145–161.

[21] D. Stevenson and H. Schaub, "Multi-Sphere Method for modeling spacecraft electrostatic forces and torques," *Adv. Space Res.*, vol. 51, no. 1, pp. 10–20, Jan. 2013.

[22] J. S. Halekas, D. L. Mitchell, R. P. Lin, L. L. Hood, M. Acuña, and A. Binder, "Evidence for negative charging of the lunar surface in shadow," *Geophys. Res. Lett.*, vol. 29, no. 10, pp. 77-1–77-4, 2002.

[23] J. S. Halekas, G. T. Delory, R. P. Lin, T. J. Stubbs, and W. M. Farrell, "Lunar prospector observations of the electrostatic potential of the lunar surface and its response to incident currents," *J. Geophys. Res., Space Phys.*, vol. 113, no. A9, 2008. doi: 10.1029/2008JA013194.

[24] J. S. Halekas, G. T. Delory, R. P. Lin, T. J. Stubbs, and W. M. Farrell, "Lunar Prospector measurements of secondary electron emission from lunar regolith," *Planet. Space Sci.*, vol. 57, no. 1, pp. 78–82, Jan. 2009.

[25] H. E. Spence *et al.*, "Science goals and overview of the radiation belt storm probes (RBSP) energetic particle, composition, and thermal plasma (ECT) suite on NASA's van allen probes mission," *Space Sci. Rev.*, vol. 179, nos. 1–4, pp. 311–336, 2013.

[26] J. McFadden *et al.*, "The THEMIS ESA plasma instrument and in-flight calibration," *Space Sci. Rev.*, vol. 141, nos. 1–4, pp. 277–302, 2008.

[27] C. Pollock *et al.*, "Fast plasma investigation for magnetospheric multiscale," *Space Sci. Rev.*, vol. 199, nos. 1–4, pp. 331–406, 2016.

[28] C. W. Carlson, J. P. McFadden, P. Turin, D. W. Curtis, and A. Magoncelli, "The electron and ion plasma experiment for fast," in *The FAST Mission*. Dordrecht, The Netherlands: Springer, 2001, pp. 33–66.

[29] C. D. Lindstrom *et al.*, "The compact environmental anomaly sensor risk reduction: A pathfinder for operational energetic charged particle sensors," *IEEE Trans. Nucl. Sci.*, vol. 65, no. 1, pp. 439–447, Jan. 2018.

[30] A. Mohammadzadeh *et al.*, "The ESA standard radiation environment monitor program first results from PROBA-I and INTEGRAL," *IEEE Trans. Nucl. Sci.*, vol. 50, no. 6, pp. 2272–2277, Dec. 2003.

[31] M. Gruss. (Jun. 2015). *Air Force Seeks Info on Space Weather Sensor*. [Online]. Available: https://spacenews.com/air-force-seeks-info-on-space-weather-sensor/

[32] E. J. Sternglass, "Theory of secondary electron emission by high-speed ions," *Phys. Rev. J. Arch.*, vol. 108, no. 1, p. 1, 1957.

[33] N. L. Sanders and G. T. Inouye, "Secondary emission effects on spacecraft charging: Energy distribution considerations," *Spacecraft Charging Technol.*, vol. 2071, p. 747, 1979.

[34] T. Kaneko, "Energy distribution of secondary electrons emitted from solid surfaces under electron bombardment: I. Theory," *Surf. Sci.*, vol. 237, nos. 1–3, pp. 327–336, 1990.

[35] H. Bruining, *Physics and Applications of Secondary Electron Emission: Pergamon Science Series: Electronics and Waves-A Series of Monographs*. Amsterdam, The Netherlands: Elsevier, 1954.

[36] M. S. Chung and T. E. Everhart, "Simple calculation of energy distribution of low-energy secondary electrons emitted from metals under electron bombardment," *J. Appl. Phys.*, vol. 45, no. 2, pp. 707–709, 1974.

[37] S. T. Lai, *Fundamentals of Spacecraft Charging: Spacecraft Interactions with Space Plasmas*. Princeton, NJ, USA: Princeton Univ. Press, 2011.

[38] C. R. Seubert, L. A. Stiles, and H. Schaub, "Effective coulomb force modeling for spacecraft in earth orbit plasmas," *Adv. Space Res.*, vol. 54, no. 2, pp. 209–220, 2014.

[39] W. R. Smythe, *Static And Dynamic Electricity*, 3rd ed. New York, NY, USA: McGraw-Hill, 1968.

[40] M. T. Bengtson and H. Schaub, "Remote sensing of spacecraft potential at geosynchronous orbit using secondary and photo electrons," in *Proc. AIAA Scitech Forum*, 2019, p. 0311.

[41] W. C. Gibson, *The Method of Moments in Electromagnetics*. London, U.K.: Chapman & Hall, Nov. 2007.
[42] E. A. Hogan and H. Schaub, "Space weather influence on relative motion control using the touchless electrostatic tractor," *J. Astron. Sci.*, vol. 63, no. 3, pp. 237–262, 2016.
[43] B. T. Draine and E. E. Salpeter, "On the physics of dust grains in hot gas," *Astrophys. J.*, vol. 231, no. 1, pp. 77–94, Jul. 1979.
[44] V. Davis, B. Gardner, M. Mandell, and K. Wilcox, *NASCAP-2k User's Manual*, 4th ed. San Diego, CA, USA: Science Applications International Corporation, Feb. 2011.
[45] A. L. Victor, T. H. Zurbuchen, and A. D. Gallimore, "Top hat electrostatic analyzer for far-field electric propulsion plume diagnostics," *Rev. Sci. Instrum.*, vol. 77, no. 1, 2006, Art. no. 013505.
[46] H. O. Funsten *et al.*, "Helium, oxygen, proton, and electron (HOPE) mass spectrometer for the radiation belt storm probes mission," *Space Sci. Rev.*, vol. 179, nos. 1–4, pp. 423–484, 2013.
[47] D. N. Baker *et al.*, "The relativistic electron-proton telescope (REPT) instrument on board the radiation belt storm probes (RBSP) spacecraft: Characterization of earth's radiation belt high-energy particle populations," in *The Van Allen Probes Mission*. New York, NY, USA: Springer, 2012, pp. 337–381.
[48] J. B. Blake *et al.*, "The fly's eye energetic particle spectrometer (FEEPS) sensors for the magnetospheric multiscale (MMS) mission," *Space Sci. Rev.*, vol. 199, nos. 1–4, pp. 309–329, 2016.
[49] R. J. L. Grard, "Properties of the satellite photoelectron sheath derived from photoemission laboratory measurements," *J. Geophys. Res.*, vol. 78, no. 16, pp. 2885–2906, 1973.

Miles Bengtson received the B.S. and M.S. degrees (Hons.) in engineering physics from Embry-Riddle Aeronautical University, Daytona Beach, FL, USA, in 2016 and 2017, respectively.

He was a Space Scholar with the Air Force Research Laboratory, Kirtland Air Force Base, Albuquerque, NM, USA. He is an Alumnus of the International Space University 2017 Space Studies Program, Cork, Ireland. He is currently a Graduate Research Assistant and a NDSEG Fellow with the Aerospace Engineering Science Department, University of Colorado at Boulder, Boulder, CO, USA. His current research interests include spacecraft-plasma interactions, charged astrodynamics, and experimentation.

Mr. Bengtson is a member of the AIAA Atmospheric and Space Environment Technical Committee.

Joe Hughes received the B.S. degree in physics and mechanical engineering from Walla Walla University, College Place, WA, USA, in 2014, and the Ph.D. degree in spacecraft charging and its effects on spacecraft orbits from the Aerospace Engineering Sciences Department, University of Colorado at Boulder, Boulder, CO, USA, in 2018. He is currently a Research Scientist with ASTRA, Louisville, CO, USA. His current research interests include spacecraft charging, electrostatics, and GPS radio occultation.

Hanspeter Schaub is currently the Glenn L. Murphy Chair of engineering with the University of Colorado at Boulder, Boulder, CO, USA, where he is also the Graduate Chair of the Aerospace Engineering Sciences Department. He has more than 20 years of research experience, of which 4 years with Sandia National Laboratories, Albuquerque, NM, USA. He has been the ADCS Lead in the CICERO Mission and the ADCS Algorithm Lead on a Mars Mission. In the last decade, he has developed the emerging field of charged astrodynamics. His current research interests include nonlinear dynamics and control, astrodynamics, relative motion dynamics, and relative motion sensing. This has led to about 137 journal and 208 conference publications, and *Analytical Mechanics of Space Systems* (3rd ed.).

Dr. Schaub is an AAS Fellow and an AIAA Associate Fellow. He was a recipient of the H. Joseph Smead Faculty Fellowship, the Provosts Faculty Achievement Award, the Faculty Assembly Award for Excellence in Teaching, the Outstanding Faculty Advisor Award, and the AIAA/ASEE Atwood Educator Award, and the AIAA Mechanics and Control of Flight Award. He currently serves as the Editor-In-Chief for the AIAA *Journal of Spacecraft and Rockets*.